

Rotational dynamics of an asymmetric top molecule in parallel electric and non-resonant laser fields

Juan J. Omiste* and Rosario González-Férez†

Instituto Carlos I de Física Teórica y Computacional, and Departamento de Física Atómica, Molecular y Nuclear, Universidad de Granada, 18071 Granada, Spain

(Dated: February 25, 2022)

We present a theoretical study of the rotational dynamics of asymmetry top molecules in an electric field and a parallel non-resonant linearly polarized laser pulse. The time-dependent Schrödinger equation is solved within the rigid rotor approximation. Using the benzonitrile molecule as prototype, we investigate the field-dressed dynamics for experimentally accessible field configurations and compare these results to the adiabatic predictions. We show that for an asymmetric top molecule in parallel fields, the formation of the pendular doublets and the avoided crossings between neighboring levels are the two main sources of non-adiabatic effects. We also provide the field parameters under which the adiabatic dynamics would be achieved.

I. INTRODUCTION

The availability of oriented molecules provides a wealth of intriguing applications in a variety of molecular sciences, such as in chemical reaction dynamics [1–5], photoelectron angular distributions [6–8], or high-order harmonic generation [9–11]. An oriented molecule is characterized by the confinement of the molecular fixed axes along the laboratory fixed axes and by its dipole moment pointing in a particular direction. Many experimental efforts have been undertaken to control the rotational degree of freedom, and in particular to orient polar molecules [1, 12–22].

Here, we focus on a theoretical study of the mixed-field orientation technique, which is based on the combination of weak dc and strong non-resonant radiative fields [19, 20]. Strongly oriented/antioriented states could be created by coupling the nearly degenerate pair of states with opposite parity forming a pendular doublet by means of a weak dc field. This theoretical prediction is based on an adiabatic picture in which the turn-on time of the laser pulse is larger than the molecular rotational period [23]. For asymmetric top molecules, a theoretical study based on a time-independent model of their mixed-field orientation pointed out that a fully adiabatic description of this process does not reproduce the experimental results [24]. We have recently found that a time-dependent description of the mixed-field orientation of linear molecules is required to explain the experimental observations [25, 26]. Two main sources of non-adiabatic effects were identified for linear molecules: i) the coupling of the levels forming quasidegenerate pendular doublets as the laser intensity is increased gives rise to a transfer of population between them; ii) the strongly coupled states from the same J manifold for tilted fields are driven apart as the laser intensity is increased in the weak-field regime, provoking a population redistribution among them. In

addition, for highly excited states, avoided crossing in the field-dressed spectrum could affect the rotational dynamics. A similar time-dependent study for polar asymmetric top molecules is desirable for a correct interpretation of the numerous mixed-field experiments with these systems [21, 27]. Compared to linear molecules, asymmetric tops possess a more dense level structure and, when the fields are turned on these levels could be strongly coupled. Thus, a more complex rotational dynamics should be expected for asymmetric tops in combined dc and ac fields. Let us also mention that several theoretical and experimental studies have investigated the relevance of non-adiabatic phenomena on the manipulation of molecules with external fields [28–34].

In this work, we perform a theoretical investigation of the rotational dynamics of an asymmetric top in parallel electric and non-resonant radiative fields within the rigid rotor description. The time-dependent Schrödinger equation is solved using experimental field configurations, i.e., first a weak electric field that is switched on at a constant speed and then a parallel linearly polarized Gaussian laser pulse is turned on. For several rotational states, we show that under ns-pulses the dynamics is not adiabatic and it is characterized by the formation of the pendular doublets and the numerous avoided crossings of the field-dressed spectrum. We have proven that due the different time scales associated to each phenomenon, it might become experimentally harder to reach the adiabatic limit. Increasing the electric field strength helps for the lowest-lying state in a certain irreducible representation; whereas for an excited one a proper combination of dc field with the temporal width of the pulse is needed to optimize the mixed-field orientation process.

The paper is organized as follows: In Sec. II we describe the Hamiltonian of the system, its symmetries and the numerical method used to solve the time-independent Schrödinger equation. The main properties of our prototype molecule benzonitrile are provided in Sec. III. In Sec. IV we investigate the mixed-field dynamics of the ground state of several irreducible representations, analogously for several excited states in Sec. V. We explore the final orientation of these states as the field parame-

* omiste@ugr.es

† rogonzal@ugr.es

ters are varied, identify the sources of non-adiabatic effects and seek for the adiabatic regime. The conclusions are given in Sec. VI.

II. THE HAMILTONIAN OF AN ASYMMETRIC TOP MOLECULE IN PARALLEL FIELDS

We consider a polar asymmetric top molecule in parallel homogeneous static electric field and non-resonant linearly polarized laser pulse. The polarization of the laser lies along the Z -axis of the laboratory fixed frame (LFF) (X, Y, Z) and the electric field is also parallel to this Z -axis. We only consider molecules with diagonal polarizability tensors, and the dipole moment parallel to the z -axis of the molecular fixed frame (MFF) (x, y, z) , and the smallest moment of inertia is parallel to the x -axis. The LFF and MFF are related by the Euler angles (θ, ϕ, χ) [35]. Within the rigid rotor approximation, the Hamiltonian reads

$$H(t) = H_R + H_s(t) + H_L(t), \quad (1)$$

where H_R stands for the field-free Hamiltonian

$$H_R = B_x J_x^2 + B_y J_y^2 + B_z J_z^2 \quad (2)$$

with J_k being the projection of the total angular momentum operator \mathbf{J} along the k -axis of the MFF with $k = x, y$ and z . The rotational constant along the MFF k -axis is $B_k = \frac{\hbar^2}{2I_{kk}}$ with I_{kk} the moment of inertia with respect to this axis k . We are using the left-handed convention I^l [36], and the rotational constant of the considered molecule satisfy $B_z > B_y > B_x$.

The interaction of the electric field $\mathbf{E}_s(t) = E_s(t)\hat{Z}$ with the permanent dipole moment, $\boldsymbol{\mu} = \mu\hat{z}$, reads

$$H_s(t) = -\boldsymbol{\mu} \cdot \mathbf{E}_s(t) = -\mu E_s(t) \cos \theta, \quad (3)$$

where $E_s(t)$ initially depends linearly on time, and once the maximum strength E_s is reached, it is kept constant. The turning on speed is chosen so that this process is adiabatic. Here, we work in the weak or moderate dc-field regime. Thus, we can neglect the coupling of this field with the molecular polarizability and higher order terms.

The interaction of the non-resonant laser field and the molecule can be written as [23]

$$H_L(t) = -\frac{I(t)}{2\epsilon_0 c} (\alpha^{zx} \cos^2 \theta + \alpha^{yx} \sin^2 \theta \sin^2 \chi), \quad (4)$$

where $\alpha^{km} = \alpha_{kk} - \alpha_{mm}$ are the polarizability anisotropies, being α_{kk} the polarizability along the molecular axis $k = x, y$ and z . ϵ_0 is the dielectric constant and c the speed of light. The intensity of the non-resonant laser pulse is $I(t)$. We analyze Gaussian pulses

Parity			Functions
$C_Z(\delta)$	σ_Z	K	
e	e	$e, K = 0$	$ J00\rangle$
e	e	$e, K \neq 0$	$\frac{1}{\sqrt{2}} (JK0\rangle + (-1)^K J-K0\rangle)$
e	o	e	$\frac{1}{\sqrt{2}} (JK0\rangle + (-1)^{K+1} J-K0\rangle)$
o	e	o	$\frac{1}{\sqrt{2}} (JK0\rangle + (-1)^K J-K0\rangle)$
o	o	o	$\frac{1}{\sqrt{2}} (JK0\rangle + (-1)^{K+1} J-K0\rangle)$

Table I. For the states with $M = 0$ in parallel fields, functions used in the basis set expansion of their wave function.

with intensity $I(t) = I_0 \exp\left(-\frac{t^2}{2\sigma^2}\right)$, I_0 is the peak intensity, which is reached at $t = 0$, and σ is related to full width half maximum (FWHM) as $\tau = 2\sqrt{2} \ln 2 \sigma$.

Based on current mixed-field orientation experiments, we assume a field-free molecule and turn on the electric field first. Once the maximum dc field strength is reached, the Gaussian pulse is switched on. Since the turning on of the dc field is adiabatic, here we investigate the non-adiabatic effects appearing in this second stage.

In this parallel field configuration, the symmetries of the rigid rotor Hamiltonian (1) are the identity, E , the two fold rotation around the MFF z -axis, arbitrary rotations around the LFF Z $C_Z(\delta)$, and the reflection on any plane containing the fields σ_Z . Then, the projection of \mathbf{J} on the Z -axis M and the parity of its projection on the z -axis, i.e., the parity of K , are good quantum numbers. For $M \neq 0$, there are four irreducible representations and the symmetry of reflection on any plane containing the fields implies the well known degeneracy in $|M|$. For $M = 0$, the wave function can have even and odd parity under these reflections, giving rise to two irreducible representations for each parity of K .

To solve the time-dependent Schrödinger equation of the Hamiltonian (1), we employ the short iterative Lanczos algorithm for the time propagation [37], and a basis set representation for the angular coordinates. The time step used in short iterative Lanczos algorithm varies from $\delta t = 3.5$ fs to $\delta t = 150$ fs for $\tau = 0.5$ ns and $\tau = 20$ ns, respectively. In our calculations, the number of vectors in the Krylov space is adapted during the time propagation to keep the error below 10^{-9} . For each irreducible representation, we construct a basis using linear combinations of the field-free symmetric top eigenfunctions $|JKM\rangle$ [35] that respect the symmetries [38]. For the states with $M = 0$, we provide in Table I the basis functions used for each irreducible representation. For the states with $M \neq 0$, the basis is formed by the functions $|JKM\rangle$ with the same parity of K .

For reasons of addressability, we label the field-dressed wave function using the field-free notation $|J_{K_a, K_c} M\rangle_t$ where K_a and K_c are the values of K on the limiting

symmetric top rotor prolate and oblate cases [36], respectively. Let us remark that we are using the left-handed convention I^l with $a = z$, $b = y$ and $c = x$. We have made explicit the dependence on time t of the wave function, but not on the field parameters I_0 , τ and E_s .

To have a better physical insight on the non-adiabatic effects of the field-dressed dynamics, the time-dependent wave function $|J_{K_a, K_c} M\rangle_t$ is expanded in the basis formed by the adiabatic basis at time t

$$|J_{K_a, K_c} M\rangle_t = \sum_{j=0}^N C_{\gamma_j}(t) |\gamma_j\rangle_p \quad (5)$$

with $C_{\gamma_j}(t) = {}_p\langle\gamma_j|J_{K_a, K_c} M\rangle_t$, and $|\gamma_j\rangle_p$ denotes the adiabatic states of Hamiltonian (1) taking the electric field strength and the laser intensities constant. Note that for each time step t , the time-independent Schrödinger equation is solved and an adiabatic basis is constructed. This pendular basis can be used to characterize as adiabatic or diabatic the time evolution of a wave function. Thus, the rotational dynamics could be considered as fully adiabatic if the criterion

$$\eta = \frac{\hbar \left| \left\langle \gamma_i \left| \frac{\partial H_L(t)}{\partial t} \right| \gamma_j \right\rangle_p \right|}{|E_i - E_j|^2} \ll 1$$

is satisfied [39].

III. THE SYSTEM

In this work, we use the benzonitrile molecule (BN) as prototype to illustrate our results. Its rotational constants are $B_x = 1214$ MHz, $B_y = 1547$ MHz and $B_z = 5655$ MHz, the permanent dipole moment $\mu = 4.515$ D and the polarizabilities are $\alpha_{xx} = 7.49$ Å³, $\alpha_{yy} = 13.01$ Å³ and $\alpha_{zz} = 18.64$ Å³ [40, 41]. For the sake of simplicity, we restrict this study to several rotational states of even parity with respect to the reflections on XZ -plane and under a π -rotation around the MFF z -axis. We stress that the observed physical phenomena also appear for levels within other irreducible representations.

We consider experimentally accessible field configurations: a linearly polarized Gaussian pulse with the FWHM in the nanosecond range and peak intensities $10^{11} \text{ W/cm}^2 \leq I_0 \leq 10^{12} \text{ W/cm}^2$; and a weak dc field similar to the one present in a velocity-mapping image spectrometer of few hundreds V/cm. Here, we assume that the dc field is switched on slowly enough to ensure an adiabatic dynamics in this first stage. In the experiment, this assumption strongly depends on the velocity of the molecules when they reach the velocity-mapping image spectrometer. If this tuning-on process is not adiabatic, before the pulse is switched on the wave function would be a superposition of several eigenstates of the

Hamiltonian (1) with $I_0 = 0 \text{ W/cm}^2$ and the maximum dc field strength E_s . As a consequence, the field-dressed dynamics could be more complex since these states could belong to different pendular doublets at strong laser intensities.

In a mixed-field orientation experiment, the measurements are done once the laser pulse has reached the peak intensity, i.e., at $t = 0$ in our theoretical model. We first analyze the rotational dynamics as the laser intensity $I(t)$ is increased. This allows us to understand the different physical phenomena giving rise to a non-adiabatic dynamics. We also investigate the orientation at the peak intensity, i.e., at $t = 0$.

IV. FIELD-DRESSED DYNAMICS OF THE GROUND STATE OF SEVERAL IRREDUCIBLE REPRESENTATIONS

We start analyzing the mixed-field orientation of the ground states of the irreducible representations with $M = 0$ and 3, i.e., the levels $|0_{0,0}0\rangle$ and $|3_{0,3}3\rangle$. We have chosen these states because in mixed-field orientation experiment of BN they have a significant population in the quantum-state selected beam [21, 27], and the knowledge of their field-dressed dynamics is important for these experiments.

A. Dynamics of the state $|0_{0,0}0\rangle_t$

In Fig. 1(a) and Fig. 1(b) we present the orientation $\langle \cos \theta \rangle$ of the ground state $|0_{0,0}0\rangle_t$ as a function of the laser intensity $I(t)$ for $E_s = 300 \text{ V/cm}$ and $E_s = 600 \text{ V/cm}$, respectively. The Gaussian pulses have $I_0 = 7 \times 10^{11} \text{ W/cm}^2$ and several FWHM. For comparison, the orientation of the adiabatic state $|0_{0,0}0\rangle_p$ is also presented. For all these field-configurations, the orientation shows a qualitatively similar behavior: $\langle \cos \theta \rangle$ monotonically increases as $I(t)$ is increased, once the pendular limit is reached, the slope of $\langle \cos \theta \rangle$ versus $I(t)$ is reduced, and $\langle \cos \theta \rangle$ increases smoothly with a value smaller than the adiabatic limit. This reduction on the final orientation is due to the non-adiabatic effects. Analogously to the ground state of a linear molecule in combined electric and non-resonant laser fields, the loss of adiabaticity in the field-dressed dynamics of $|0_{0,0}0\rangle_t$ is due to the formation of the quasidegenerate pendular doublets [26]. Thus, increasing the FWHM of the pulse will increase the orientation [25, 26, 42, 43]. In Fig. 2, we present how the pendular doublet between the adiabatic states $|0_{0,0}0\rangle_p$ and $|1_{0,1}0\rangle_p$ is formed. To illustrate this loss of adiabaticity of $|0_{0,0}0\rangle_t$ we show the population of the adiabatic ground state $|0_{0,0}0\rangle_p$, $|C_{0_{0,0}0}(t)|^2$, in Fig. 3. Note that for the ground state, $|C_{0_{0,0}0}(t)|^2 + |C_{1_{0,1}0}(t)|^2 = 1$. For $E_s = 300 \text{ V/cm}$, the rotational dynamics is adiabatic if the pulse has $\tau \geq 4 \text{ ns}$, whereas for smaller values of τ the

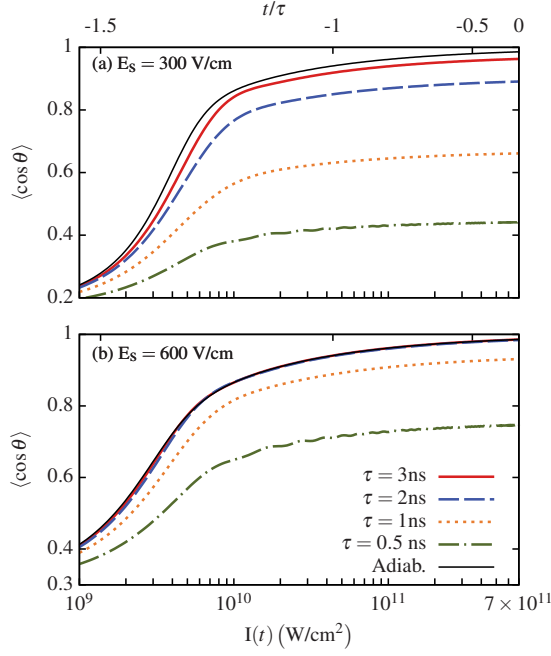


FIG. 1. (Color online) For the absolute ground state $|0_{0,0}0\rangle_t$, we present the expectation value $\langle \cos \theta \rangle$ versus the laser intensity $I(t)$ for (a) $E_s = 300$ V/cm and (b) $E_s = 600$ V/cm. The peak intensity is $I_0 = 7 \times 10^{11}$ W/cm² and the FWHM are $\tau = 3$ ns (red solid), $\tau = 2$ ns (blue long dashed), $\tau = 1$ ns (orange dotted) and $\tau = 0.5$ ns (green dashed-dotted).

population transfer when the pendular doublet is formed could be very large. Using a 1 ns pulse, the population of the adiabatic ground state is $|C_{0_{0,0}0}(t)|^2 = 0.835$ at $t = 0$, and due to the contribution of the anti-oriented state $|1_{0,1}0\rangle_p$, the orientation at $t = 0$ of $|0_{0,0}0\rangle_0$ is reduced to $\langle \cos \theta \rangle = 0.661$. By increasing the dc field strength to $E_s = 600$ V/cm, the energy splitting of the pendular doublets is increased, and a Gaussian pulse of $\tau = 2$ ns already gives rise to an adiabatic dynamics for $|0_{0,0}0\rangle_t$. For a short pulse of 500 ps, the ground state is still strongly oriented with $\langle \cos \theta \rangle = 0.747$ and the contribution of the adiabatic ground state at $t = 0$ is $|C_{0_{0,0}0}(0)|^2 = 0.878$. For both dc fields and 500 ps, $\langle \cos \theta \rangle$ shows an oscillatory behavior as $I(t)$ is increased, which is due to the coupling between the two adiabatic states involved in the dynamics, i.e., the mixing term ${}_p\langle 0_{00}0 | \cos \theta | 1_{01}0 \rangle_p$.

The lowest-lying state in the irreducible representations with $M = 1$, $|1_{0,1}1\rangle_t$, is relatively well separated of neighboring levels with the same symmetry. Thus, its field-dressed dynamics shows analogous features as those discussed above for the $|0_{0,0}0\rangle_t$, and the formation of the pendular pair is the only effect provoking the loss of adiabaticity. Indeed, for $E_s = 300$ V/cm, a Gaussian pulse with $I_0 = 7 \times 10^{11}$ W/cm² and $\tau = 5$ ns gives rise to an adiabatic dynamics for this state.

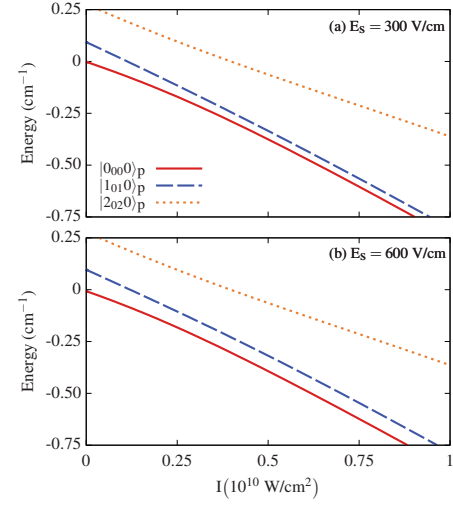


FIG. 2. (Color online) We present the formation of the pendular doublet between the states $|0_{0,0}0\rangle_p$ and $|1_{0,1}0\rangle_p$ in the adiabatic spectrum for dc field strengths (a) $E_s = 300$ V/cm and (b) $E_s = 600$ V/cm.

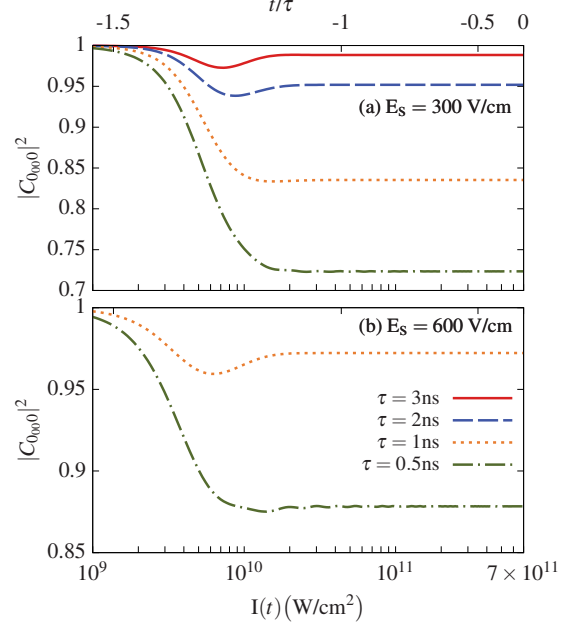


FIG. 3. (Color online) For the state $|0_{0,0}0\rangle_t$, we present the squares of the projection of the time-dependent wave function onto the adiabatic ground state $|0_{0,0}0\rangle_p$ versus the laser intensity $I(t)$ for dc field strengths (a) $E_s = 300$ V/cm and (b) $E_s = 600$ V/cm. The Gaussian pulse has $I_0 = 7 \times 10^{11}$ W/cm² and $\tau = 3$ ns (solid red), $\tau = 2$ ns (blue long dashed), $\tau = 1$ ns (orange dotted) and $\tau = 0.5$ ns (green dashed-dotted).

B. Dynamics of the state $|3_{0,3}3\rangle_t$

For higher values of M , the avoided crossings leave their fingerprints in the field-dressed dynamics of the corresponding ground state. As an example, we show in Fig. 4 the orientation cosine of $|3_{0,3}3\rangle_t$ for $E_s = 300$ V/cm

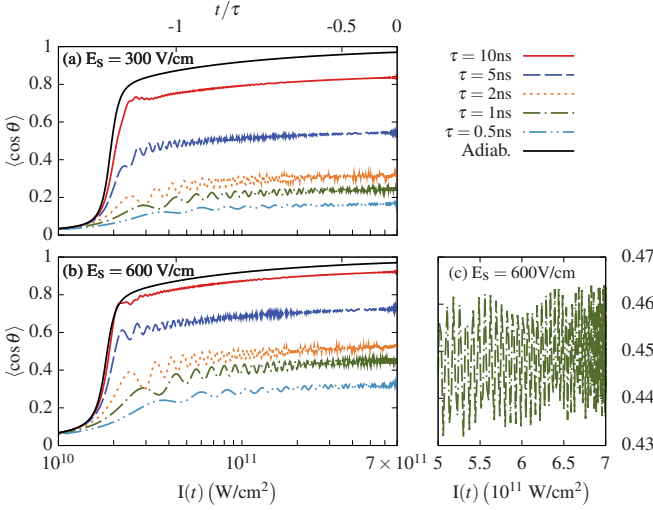


FIG. 4. (Color online) For the state $|30,3\rangle_t$, we present the orientation cosine $\langle \cos \theta \rangle$ as a function of $I(t)$ for (a) $E_s = 300$ V/cm and (b) 600 V/cm. A detail of the oscillations of $\langle \cos \theta \rangle$ for 600 V/cm is shown in panel (c). The peak intensity of the pulses is $I_0 = 7 \times 10^{11}$ W/cm 2 , and the FWHM are $\tau = 10$ ns (red solid line), $\tau = 5$ ns (dark blue long dashed line), $\tau = 2$ ns (orange dotted line), $\tau = 1$ ns (dark olive green dot-dashed line), $\tau = 0.5$ ns (light blue double-dot-dashed line). The adiabatic results are also shown (black solid line).

and $E_s = 600$ V/cm, the adiabatic value of $\langle \cos \theta \rangle$ is also included. Comparing these results to those of the absolute ground state $|00,0\rangle_t$ in Fig. 1, two main differences are encountered. First, $\langle \cos \theta \rangle$ initially increases as $I(t)$ is increased, and once the pendular doublet is formed $\langle \cos \theta \rangle$ oscillates around a mean value. Second, even the 10 ns Gaussian pulses do not ensure an adiabatic dynamics for both dc field strengths. For instance, at $t = 0$ we obtain $\langle \cos \theta \rangle = 0.921$ for $E_s = 600$ V/cm and $\tau = 10$ ns, whereas the adiabatic value is $\langle \cos \theta \rangle = 0.970$. As the FWHM is increased, the amplitude of the oscillations of $\langle \cos \theta \rangle$ is reduced.

The oscillations in the evolution of $\langle \cos \theta \rangle$ can be explained due to the coupling between the adiabatic states contributing to the dynamics. The presence of avoided crossings in the spectrum provokes that adiabatic states from different pendular doublets are populated during the rotational dynamics of $|30,3\rangle_t$. In Fig. 5(a) and Fig. 5(b), we plot the population of the pendular adiabatic states for $E_s = 300$ V/cm, $I_0 = 7 \times 10^{11}$ W/cm 2 and $\tau = 2$ ns and 5 ns, respectively. We start analyzing in detail the results for $\tau = 2$ ns. To rationalize the population redistribution taking place around $I(t) \approx 2 \times 10^{10}$ W/cm 2 , see Fig. 5(a), we present a detail of the adiabatic level structure in Fig. 6(a). As the pendular doublet between the adiabatic levels $|30,3\rangle_p$ and $|40,4\rangle_p$ is formed, $|40,4\rangle_p$ suffers an avoided crossing with $|32,2\rangle_p$. For the states $|30,3\rangle_p$ and $|40,4\rangle_p$ in the pendular doublet, the maximum value of adiabatic parameter is $\eta \approx 1.3$. The maximum of η for the

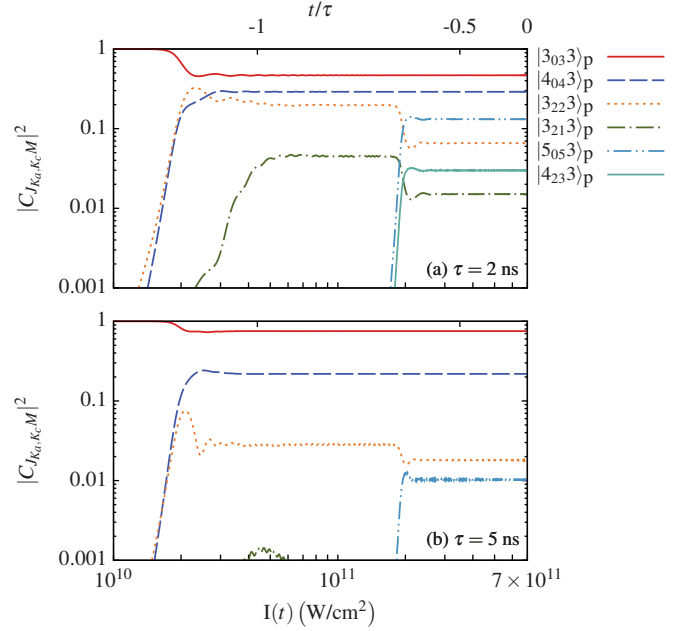


FIG. 5. (Color online) For the state $|30,3\rangle_t$, we present the squares of the projections of the time dependent wave function onto the adiabatic states versus the laser intensity $I(t)$. The Gaussian pulse has $I_0 = 7 \times 10^{11}$ W/cm 2 and (a) $\tau = 5$ ns and (b) $\tau = 2$ ns, and the dc field strength is $E_s = 300$ V/cm.

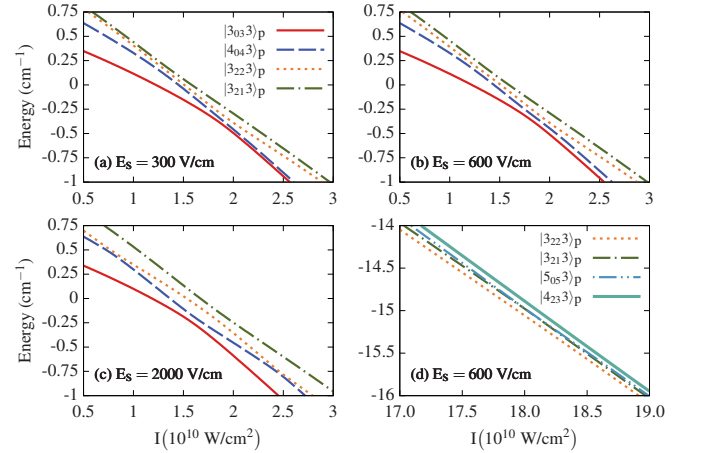


FIG. 6. (Color online) (a), (b) and (c) Adiabatic energy structure when the pendular doublets between the states $|30,3\rangle_p$ and $|40,4\rangle_p$ is formed for $E_s = 300$ V/cm, $E_s = 600$ V/cm and $E_s = 2$ kV/cm, respectively. (d) Avoided crossing between the adiabatic states $|32,2\rangle_p$, $|32,1\rangle_p$, $|50,5\rangle_p$ and $|42,3\rangle_p$.

state $|32,2\rangle_p$ with $|30,3\rangle_p$ and $|40,4\rangle_p$ are $\eta \approx 0.44$ and 0.46 respectively. Thus, the two oriented states $|30,3\rangle_p$ and $|32,2\rangle_p$ are also coupled, even if their energy separation is larger. These values of η indicate that the dynamics in this region is not adiabatic. Indeed, the population of these two states $|40,4\rangle_p$ and $|32,2\rangle_p$ simultaneously increases as the one of $|30,3\rangle_p$ decreases. Once the pendular pair between $|30,3\rangle_p$ and

$|4_{0,4}\rangle_p$ is formed their populations keep a constant behavior as $I(t)$ is increased. We observe the formation of the second pendular doublet in this irreducible representation for $I(t) \approx 3 \times 10^{10} \text{ W/cm}^2$: the population of the adiabatic states $|3_{2,2}\rangle_p$ and $|3_{2,1}\rangle_p$ decreases and increases, respectively. By further increasing $I(t)$ the states $|3_{2,2}\rangle_p$ and $|3_{2,1}\rangle_p$ suffer an avoided crossing with those from the third pendular doublet $|5_{0,5}\rangle_p$ and $|4_{2,3}\rangle_p$, see Fig. 6(d). Through this avoided crossing, there is a strong coupling between the oriented states $|3_{2,2}\rangle_p$ and $|5_{0,5}\rangle_p$ with the adiabatic parameter reaching the maximum value $\eta \approx 1.93$, and between the antioriented ones $|3_{2,1}\rangle_p$ and $|4_{2,3}\rangle_p$ with $\eta \approx 1.92$. In both cases the dynamics is not adiabatic, and we observe in Fig. 5(a) how their populations are interchanged around $I(t) \approx 2 \times 10^{11} \text{ W/cm}^2$. The oscillations in $\langle \cos \theta \rangle$ are due to the coupling between all these adiabatic states that are populated. As the laser intensity is increased, these levels achieve the pendular regime and these crossed matrix elements between states in the same pendular pair, i. e., ${}_p \langle 3_{03} | \cos \theta | 4_{04} \rangle_p$, ${}_p \langle 3_{22} | \cos \theta | 3_{21} \rangle_p$ and ${}_p \langle 5_{05} | \cos \theta | 4_{23} \rangle_p$, approach zero. As t increases, the frequency of the oscillation varies because different pendular adiabatic states dominate the field-dressed dynamics, see Fig. 4(c). At $t = 0$, the field-dressed wave function of the state $|3_{0,3}\rangle_0$ has significant contributions from 6 different adiabatic states, which gives rise to a weak orientation $\langle \cos \theta \rangle = 0.327$. For $\tau = 5 \text{ ns}$, the dynamics is more adiabatic. Thus, when the pendular doublets are formed the interchange of population is smaller than for a $\tau = 2 \text{ ns}$ pulse, see Fig. 5(b). The avoided crossing are not crossed adiabatically. Indeed, the population of the states $|3_{2,1}\rangle_p$ and $|4_{2,3}\rangle_p$ is smaller than 0.001, and the field-dressed dynamics of $|3_{0,3}\rangle_t$ is dominated by the adiabatic states $|3_{0,3}\rangle_p$, $|4_{0,4}\rangle_p$, $|3_{2,2}\rangle_p$ and $|5_{0,5}\rangle_p$. This explain that the oscillations of $\langle \cos \theta \rangle$ are reduced, and that at $t = 0$ this state shows a significant orientation with $\langle \cos \theta \rangle = 0.547$.

For other ground states, such as $|2_{0,2}\rangle_t$ and $|4_{0,4}\rangle_t$, we have encountered similar phenomena, and their rotational dynamics is strongly dominated by avoided crossings.

C. Influence of FWHM of the Gaussian pulse

We consider now the ground states of the irreducible representations with $M \leq 4$, that is the states $|0_{0,0}\rangle_t$, $|1_{0,1}\rangle_t$, $|2_{0,2}\rangle_t$, $|3_{0,3}\rangle_t$ and $|4_{0,4}\rangle_t$. In this section we investigate the impact of the temporal width of the Gaussian pulse on their rotational dynamics. Their orientation at the peak intensity, i. e., at $t = 0$, are plotted versus τ in Fig. 7(a) and Fig. 7(b) for $E_s = 300 \text{ V/cm}$ and $E_s = 600 \text{ V/cm}$, respectively. The peak intensity is fixed to $I_0 = 7 \times 10^{11} \text{ W/cm}^2$.

In contrast to the mixed-field orientation of a linear molecules [26], a smaller field-free rotational energy

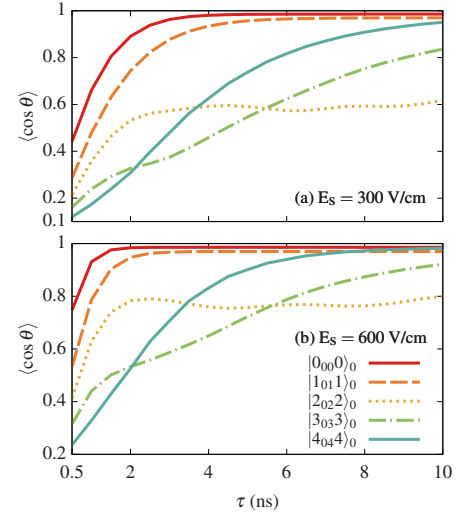


FIG. 7. (Color online) For the ground states of several irreducible representations, we plot the expectation value $\langle \cos \theta \rangle$ at $t = 0$ as a function of the FWHM of the Gaussian pulse for (a) $E_s = 300 \text{ V/cm}$ and (b) $E_s = 600 \text{ V/cm}$. The peak intensity is fixed to $I_0 = 7 \times 10^{11} \text{ W/cm}^2$.

does not imply a larger orientation. For instance, using $E_s = 300 \text{ V/cm}$, the state $|4_{0,4}\rangle_0$ shows a larger orientation than $|2_{0,2}\rangle_0$ and $|3_{0,3}\rangle_0$ for $\tau \gtrsim 2 \text{ ns}$ and 3.5 ns , respectively. For $\tau \gtrsim 6 \text{ ns}$, the state $|2_{0,2}\rangle_0$ is the least oriented. As indicated above, the non-adiabatic features of the field-dressed dynamics are due to the formation of the pendular doublets and to the avoided crossings. By increasing τ , we can ensure that less population is transferred from the oriented state to the antioriented one or vice-versa as the pendular doublet is formed. However, the characteristic time scale of the avoided crossings is different, and significantly larger FWHM are needed to pass them adiabatically. Each irreducible representation is characterized by a certain field-dressed level structure, and, therefore, by an amount of avoided crossings which contribute to the complexity of the rotational dynamics. The absence of avoided crossings close to the ground states gives rise to a monotonic increase of $\langle \cos \theta \rangle$ approaching the adiabatic limit as τ is increased, this behavior is observed in the levels $|0_{0,0}\rangle_t$ and $|1_{0,1}\rangle_t$. In contrast, the influence of an avoided crossing in the dynamics implies that significantly longer pulses are needed to reach the adiabatic limit, e. g., the levels $|2_{0,2}\rangle_t$ and $|3_{0,3}\rangle_t$. In particular, for $\tau \gtrsim 2 \text{ ns}$, the orientation $\langle \cos \theta \rangle$ of $|2_{0,2}\rangle_t$ shows a smooth oscillatory behavior as a function of τ .

D. Influence of electric-field strength

In this section, we consider the same set of ground states and analyze their orientation at $t = 0$ as a function of the dc field strength, see Fig. 8. For a given laser pulse, the largest is the energy gap between the two levels in a

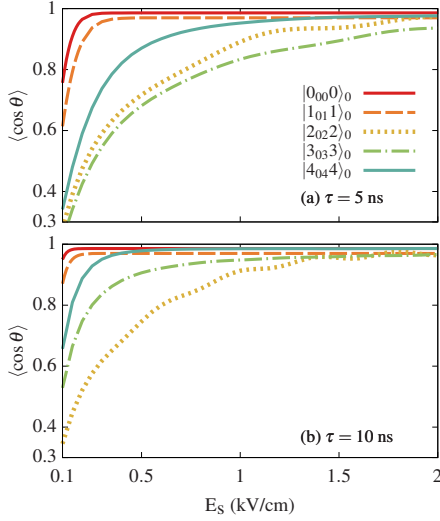


FIG. 8. (Color online) For the ground states of several irreducible representations, we present their expectation value $\langle \cos \theta \rangle$ once the peak intensity is reached at $t = 0$ as a function of the dc field strength E_s for (a) $\tau = 5$ ns and (b) $\tau = 10$ ns. The peak intensity is fixed to $I_0 = 7 \times 10^{11}$ W/cm 2 .

pendular pair, the less efficient is the population transfer when the doublet is formed [26]. This statement also holds for asymmetric top molecules. However, the impact of the electric field on the avoided crossings will influence the rotational dynamics. For both pulses, we encounter that the states $|2_{0,2}2\rangle_0$ and $|3_{0,3}3\rangle_0$ present a smaller orientation than $|4_{0,4}4\rangle_0$. The level $|3_{0,3}3\rangle_0$ is more (less) oriented than $|2_{0,2}2\rangle_0$ for the $\tau = 10$ ns ($\tau = 5$ ns) pulses. Our calculations show that for these ground states, the adiabatic pendular limit could be reached using a strong electric field and a 10 ns pulse, see Fig. 8 (b).

V. FIELD-DRESSED DYNAMICS OF EXCITED STATES

In this section we analyze the mixed-field dynamics of two excited rotational states from different irreducible representations. The field-dressed spectrum is characterized by a high density of adiabatic states and a large number of avoided crossings between neighboring levels. As a consequence, the rotational dynamics is more complex, and it is harder to achieve the diabatic limit.

A. Dynamics of the state $|4_{0,4}3\rangle_t$

As a first example, we investigate the dynamics of the rotational state $|4_{0,4}3\rangle_t$ which forms the pendular pair with $|3_{0,3}3\rangle_t$. In Fig. 9(a) and Fig. 9(b) the orientation of $|4_{0,4}3\rangle_t$ is plotted versus $I(t)$ for (a) $E_s = 300$ V/cm and (b) $E_s = 600$ V/cm, respectively. In contrast to the case of a linear molecule in parallel dc and ac fields, this

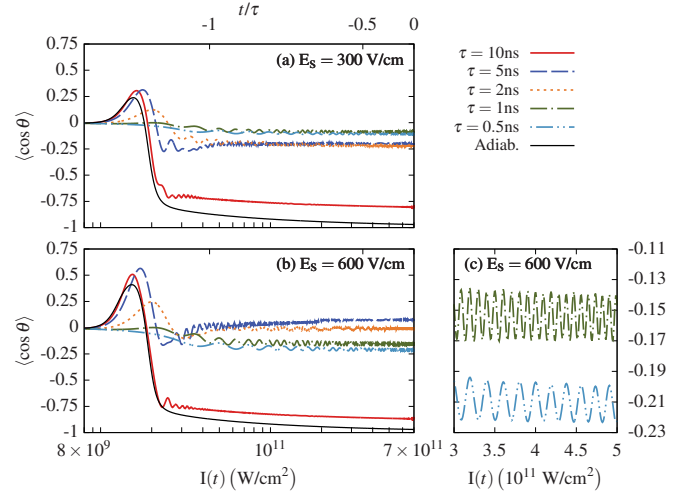


FIG. 9. (Color online) For the state $|4_{0,4}3\rangle_t$, we present $\langle \cos \theta \rangle$ versus $I(t)$ for (a) $E_s = 300$ V/cm and (b) 600 V/cm. A detail of the oscillations of $\langle \cos \theta \rangle$ for 600 V/cm is shown in panel (c). The peak intensity of the pulses is $I_0 = 7 \times 10^{11}$ W/cm 2 , and the FWHM are $\tau = 10$ ns (red solid line), 5 ns (dark blue long dashed line), 2 ns (orange dotted line), 1 ns (dark olive green dot-dashed line), 0.5 ns (light blue double-dot-dashed line). The adiabatic results is also plotted (black solid line).

state does not show the same orientation but in opposite direction as its partner in the pendular doublet the level $|3_{0,3}3\rangle_t$, except if the dynamics is adiabatic or very close to it. This can be explained in terms of the avoided crossings, which affect in different ways the rotational dynamics of $|3_{0,3}3\rangle_t$ and $|4_{0,4}4\rangle_t$. We present in Fig. 10(a) and Fig. 10(b) the contributions of adiabatic states to the rotational dynamics of $|4_{0,4}3\rangle_t$ for a 5 ns pulse with $E_s = 300$ V/cm and 600 V/cm, respectively. For both dc field strengths, we observe that the population redistribution starts first to the adiabatic states $|3_{2,2}3\rangle_p$ and $|3_{2,1}3\rangle_p$. Due to the rotational constants of BN, the states $|3_{2,2}3\rangle_p$ and $|3_{2,1}3\rangle_p$ are quasi-degenerate in energy in the absence of the fields, and as $I(t)$ varies they possess a very close energy, see Fig. 6(a) and Fig. 6(b). As a consequence, population is initially transferred to both levels, but more to $|3_{2,2}3\rangle_p$ which lies closer to $|4_{0,4}3\rangle_p$. For a stronger laser intensity, the pendular pair $|3_{0,3}3\rangle_p$ and $|4_{0,4}3\rangle_p$ starts to form and $|C_{3_{0,3}3}(t)|^2$ increases. The main difference between both dc field strengths is that for $E_s = 300$ V/cm, $|3_{0,3}3\rangle_p$ acquires the largest population; whereas for $E_s = 600$ V/cm is $|3_{2,2}3\rangle_p$. Indeed, at the largest dc field the avoided crossing is passed less adiabatically, and more population is transferred to the $|3_{2,2}3\rangle_p$, because the coupling between the states is larger. Whereas for $E_s = 600$ V/cm, the pendular pair among $|3_{0,3}3\rangle_p$ and $|4_{0,4}3\rangle_p$ is formed more adiabatically because the energy splitting in the doublets is larger, and $|3_{0,3}3\rangle_p$ is less populated than for $E_s = 300$ V/cm. In these plots, we also observe how the second pendular

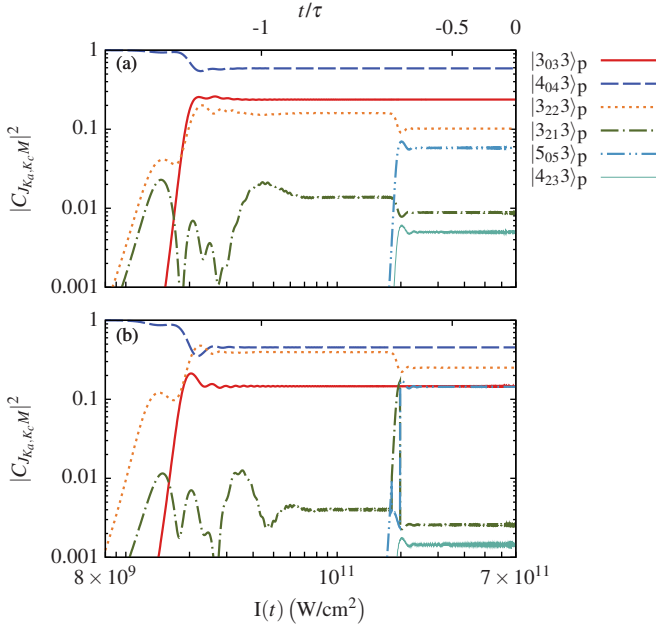


FIG. 10. (Color online) For the state $|4_{0,4}3\rangle_t$, we present the squares of the projections of the time dependent wave function onto several adiabatic states versus the laser intensity $I(t)$ for dc field strengths (a) $E_s = 300$ V/cm and (b) $E_s = 600$ V/cm. The Gaussian pulse has $I_0 = 7 \times 10^{11}$ W/cm² and $\tau = 5$ ns. The notation and label of the adiabatic states is the same as in Fig. 5.

doublet between $|3_{2,2}3\rangle_p$ and $|3_{2,1}3\rangle_p$ is formed around $I(t) \approx 2.3 \times 10^{10}$ W/cm². For stronger laser intensities, the next pendular pair $|5_{0,5}3\rangle_p$ and $|4_{2,3}3\rangle_p$ is also populated due to the avoided crossing that these levels suffer with those forming the second doublet, see Fig. 6(d). The couplings between these six pendular states provoke the oscillatory behavior of $\langle \cos \theta \rangle$. Let us mention that the first avoided crossing is not crossed adiabatically using a 10 ns pulse, but the population of the state $|3_{2,2}3\rangle_p$ is smaller than 0.03 at $t = 0$ for both field strengths. Only these 10 ns pulses give rise to a significant antiorientation with values close to the adiabatic predictions.

We investigate now the rotational dynamics of this state as the dc field is increased. For four Gaussian pulses with $I_0 = 7 \times 10^{11}$ W/cm², the orientation of $|4_{0,4}3\rangle_0$ at $t = 0$ is plotted versus E_s in Fig. 11. For this state, the adiabatic prediction is $\langle \cos \theta \rangle = -0.970$, which is independent of E_s . Our time-dependent calculations show that the orientation oscillates as E_s is increased. This behavior can be explained in terms of the avoided crossings, and their evolution as E_s varies. At $E_s = 300$ V/cm, the pendular states $|4_{0,4}3\rangle_p$ and $|3_{2,2}3\rangle_p$ suffer an avoided crossing for $I(t) \approx 1.53 \times 10^{10}$ W/cm², before the pendular doublet $|3_{0,3}3\rangle_p$, $|4_{0,4}3\rangle_p$ is formed, see Fig. 6(a). By increasing E_s , this avoided crossing is split into two, e.g., for $E_s = 2$ kV/cm, the first and second one appear at $I(t) \approx 7.8 \times 10^9$ W/cm² and $I(t) \approx 2.1 \times 10^{10}$ W/cm², respectively, and the minimal energy

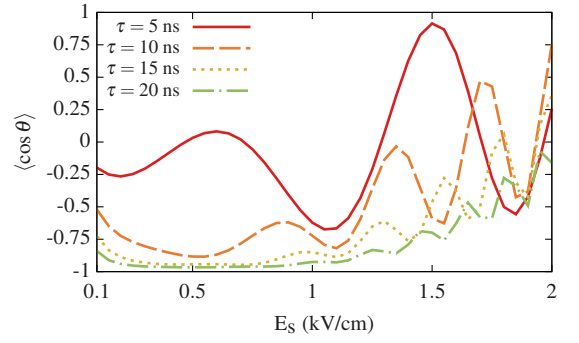


FIG. 11. (Color online) For the state $|4_{0,4}3\rangle_0$, we show the orientation at $t = 0$ versus the electric field strength E_s , for a laser pulse with $I_0 = 7 \times 10^{11}$ W/cm² and several FWHM.

between the two states in the pendular doublet is reached at $I(t) \approx 2.47 \times 10^{10}$ W/cm², see Fig. 6(c). The rotational dynamics through these avoided crossings as $I(t)$ is varied strongly depends on the FWHM of the laser pulse. For instance, using a 10 ns pulse and $E_s = 2$ kV/cm, these two avoided crossings are passed non-adiabatically and the pendular level $|3_{2,2}3\rangle_p$ is populated, and the formation of the two pendular doublets $|3_{0,3}3\rangle_p$, $|4_{0,4}3\rangle_p$ and $|3_{2,2}3\rangle_p$, $|3_{2,1}3\rangle_p$ is also non-adiabatic. Furthermore, the next avoided crossing between the pendular states $|3_{2,1}3\rangle_p$ and $|5_{0,5}3\rangle_p$, see Fig. 6(d), is also crossed non-adiabatically. Hence, the final orientation of $|4_{0,4}3\rangle_0$ strongly depends on the rotational dynamics through these avoided crossings. Indeed, as E_s is increased the population redistribution through these avoided crossings is increased; whereas less population is transferred when the pendular doublets are formed as occurs in linear molecules. For this state, to reach an adiabatic dynamics through the avoided crossings, longer laser pulses are needed, but the dc field should be chosen properly. For instance, a 20 ns pulse ensures an adiabatic dynamics of this state with 300 V/cm $\lesssim E_s \lesssim 1$ kV/cm, whereas for stronger dc fields, it is still non-adiabatic.

B. Dynamics of the state $|3_{0,3}1\rangle_t$

As a second example, we have chosen the state $|3_{0,3}1\rangle_t$, which in the field-free case is the third one with $M = 1$ and even parity under π rotation around the fields. The orientation cosine of $|3_{0,3}1\rangle_t$ is presented in Fig. 12 for several Gaussian pulses. For $E_s = 300$ V/cm, doubling the FWHM from 5 ns to 10 ns does not provoke an enhancement on the orientation. Analogously, using $E_s = 600$ V/cm, the pulses with $\tau = 2$ ns, 5 ns and 10 ns give rise to a similar orientation at $t = 0$. The dynamics of $|3_{0,3}1\rangle_t$ is strongly affected by the adiabatic states $|2_{2,1}1\rangle_p$ and $|2_{2,0}1\rangle_p$. The adiabatic state $|3_{0,3}1\rangle_p$ undergoes an avoided crossing with $|2_{2,1}1\rangle_p$, see Fig. 13, just before they form the second pendular pair in this irreducible representation. The field-free states $|2_{2,1}1\rangle$ and

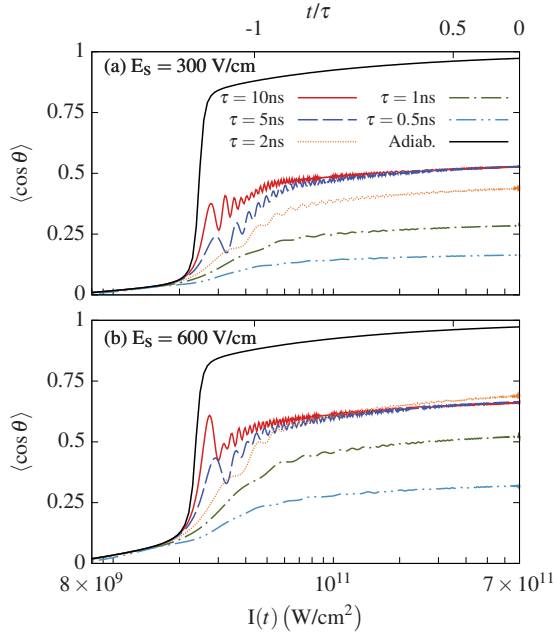


FIG. 12. (Color online) For the state $|3_{0,3}1\rangle_t$, we plot $\langle \cos \theta \rangle$ versus $I(t)$ for (a) $E_s = 300$ V/cm and (b) $E_s = 600$ V/cm. The peak intensity of the pulses is $I_0 = 7 \times 10^{11}$ W/cm², and the FWHM are $\tau = 10$ ns (red solid line), $\tau = 5$ ns (dark blue long dashed line), $\tau = 2$ ns (orange dotted line), $\tau = 1$ ns (dark olive green dot-dashed line), $\tau = 0.5$ ns (light blue double-dot-dashed line). The adiabatic results are also shown (black solid line).

$|2_{2,0}1\rangle$ are quasi-degenerate in energy, and in the presence of the fields, their energies remain very close as $I(t)$ is varied if the electric field is weak. For $E_s = 300$ V/cm, when the pendular doublet between $|3_{0,3}1\rangle_p$ and $|2_{2,1}1\rangle_p$ is formed, $|2_{2,0}1\rangle_p$ is energetically very close and the levels $|2_{2,1}1\rangle_p$ and $|2_{2,0}1\rangle_p$ suffer an avoided crossing, see Fig. 13. The population redistribution is illustrated in Fig. 14 for the Gaussian pulse with $\tau = 10$ ns and the two dc field strengths. Due to the avoided crossing between $|3_{0,3}1\rangle_p$ and $|2_{2,1}1\rangle_p$, $|C_{2_{2,1}1}(t)|^2$ achieves a first maximum as a function of $I(t)$, and afterwards it reaches a constant value once the pendular doublet is formed. As $I(t)$ is increased, the second avoided crossing between $|2_{2,1}1\rangle_p$ and $|2_{2,0}1\rangle_p$ is encountered, and the adiabatic level $|2_{2,0}1\rangle_p$ acquires a similar population as $|2_{2,1}1\rangle_p$, and they get their population almost simultaneously for $E_s = 300$ V/cm. The dynamics of $|3_{0,3}1\rangle_t$ is dominated by the adiabatic states $|3_{0,3}1\rangle_p$, $|2_{2,1}1\rangle_p$ and $|2_{2,0}1\rangle_p$. Since the last two states have similar population and they are oriented in opposite directions, the final orientation at $t = 0$ of $|3_{0,3}1\rangle_0$ is significantly smaller than the adiabatic prediction. The oscillations of $\langle \cos \theta \rangle$ are due to the couplings between these three pendular states.

Finally, we investigate the rotational dynamics of this state $|3_{0,3}1\rangle_t$ as the dc field strength is increased for sev-

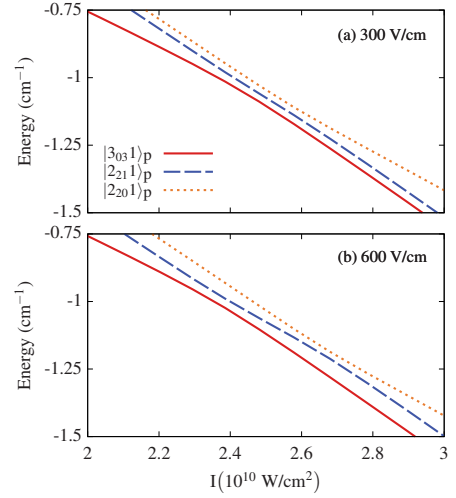


FIG. 13. We show the adiabatic level structure when the pendular doublet between the states $|3_{0,3}1\rangle_p$ and $|2_{2,1}1\rangle_p$ is formed for (a) $E_s = 300$ V/cm and (b) $E_s = 600$ V/cm.

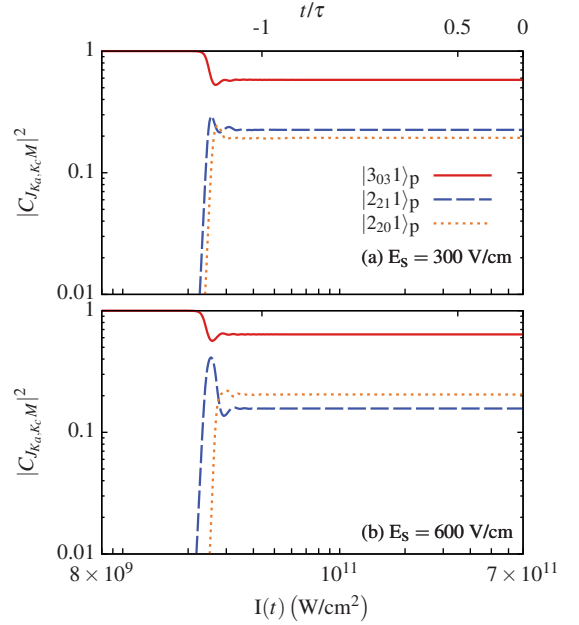


FIG. 14. (Color online) For the state $|3_{0,3}1\rangle_t$, we show the squares of the projections of the time dependent wave function onto several adiabatic states versus the laser intensity $I(t)$ for dc field strengths (a) $E_s = 300$ V/cm and (b) $E_s = 600$ V/cm. The Gaussian pulse has $I_0 = 7 \times 10^{11}$ W/cm² and $\tau = 10$ ns.

eral FWHM and $I_0 = 7 \times 10^{11}$ W/cm². The orientation cosine is presented in Fig. 15. For the four Gaussian pulses, $\langle \cos \theta \rangle$ monotonically increases as E_s is enhanced. However, even the field parameters $\tau = 20$ ns and $E_s = 2$ kV/cm do not give rise to a fully adiabatic dynamics; our time-dependent calculations provide $\langle \cos \theta \rangle = 0.956$, which is smaller than the adiabatic limit $\langle \cos \theta \rangle = 0.973$. Note that the adiabatic value is independent of E_s . An important feature of this state

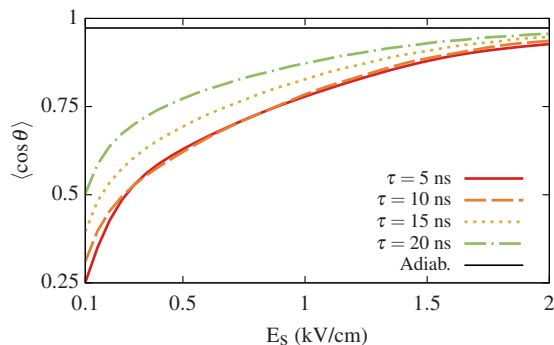


FIG. 15. (Color online) For the state $|3_{0,31}\rangle_0$, we show the orientation at $t = 0$ versus the electric field strength E_s , for a laser pulse with $I_0 = 7 \times 10^{11}$ W/cm² and several FWHM.

is that using weak dc fields, the dynamics is not adiabatic even if the FWHM is increased up to 20 ns. This lack of adiabaticity is again explained in terms of the rotational dynamics through the avoided crossings. The avoided crossing involving the adiabatic states $|3_{0,31}\rangle_p$ and $|2_{2,11}\rangle_p$ is crossed diabatically even for $\tau = 20$ ns and $E_s \leq 2$ kV/cm. The second avoided crossing among $|2_{2,11}\rangle_p$ and $|2_{2,01}\rangle_p$ is again passed non-adiabatically for these field configurations, and $|2_{2,01}\rangle_p$ acquires population. By increasing the dc field strength, the population of the state $|2_{2,01}\rangle_p$ at $t = 0$ is also increased. For sufficiently strong dc field, the dynamics of $|3_{0,31}\rangle_t$ is dominated by the adiabatic states $|3_{0,31}\rangle_p$ and $|2_{2,01}\rangle_p$, and the population of $|2_{2,11}\rangle_p$ is reduced. Since $|3_{0,31}\rangle_p$ and $|2_{2,01}\rangle_p$ are right-way oriented in the pendular regime, $\langle \cos \theta \rangle$ shows a smooth increasing behaviour as a function of E_s . For this state, the adiabatic dynamics is reached only if long enough Gaussian pulses are used, and increasing the dc field strengths will facilitate to reach this adiabatic limit.

VI. CONCLUSIONS

In this work, we have investigated the impact of parallel dc fields and non-resonant laser pulses on an asymmetric top molecule. For several rotational levels, we have explored in detail their rotational dynamics as the intensity of the laser pulse is increased till its peak value. Such a study has allowed us to identify the sources of non-adiabatic effects and the regime when they appear. In addition, we have analyzed the degree of orientation as the FWHM of the Gaussian pulse and the electric field strength are varied.

We have encountered only a few rotational states, such as $|0_{0,0}\rangle_t$ and $|1_{0,11}\rangle_t$, for which the field-dressed dynamics is dominated by the formation of the pendular pairs. For other states, the dynamics is more complicated because the time evolution of their wave function is strongly affected by the avoided crossings. At the ac

field regime where the pendular doublets are formed, the presence of additional avoided crossings provokes the interaction between three or even more adiabatic levels. In such a region, the complexity of these avoided crossings prevent us from using the Landau-Zener criteria or a two state model to analyze the rotational dynamics through them. The avoided crossings give rise to a highly non-adiabatic dynamics, and the final degree of orientation could be reduced. We have shown that dc fields with strengths up to 2 kV/cm do not ensure an adiabatic dynamics for low-lying rotational states. Thus, the path to the adiabaticity necessitates laser pulses with longer temporal widths. Due to the different time scales associated to both phenomena, the pendular doublet formation and avoided crossings, the field configuration required to achieve an adiabatic dynamics simultaneously for many rotational states becomes harder to produce experimentally. A laser pulse could be designed with a small slope of the intensity in the field regime where most of the avoided crossings appear and pendular doublet are formed, trying to minimize the population redistribution at that region. So that, the degree of adiabaticity could be significantly enhanced.

In this work, we have analyzed the field-dressed dynamics of benzonitrile, but the above-observed physical phenomena are expected to occur in other polar asymmetric top molecules. Due to the complex structure of these systems, a similar theoretical study should be performed for each specific molecule. The field regime under which the adiabatic dynamics would be achieved strongly depends on the rotational constant, the polarizability tensor and the permanent dipole moment.

A natural extension to this work would be the investigation of an asymmetric top molecule in a nonparallel field configuration, as those used in the mixed-field orientation experiments [21, 27]. For tilted fields, the complexity of the field-dressed level structure is enhanced due to the presence of avoided crossings between states having different field-free magnetic quantum numbers. Due to this new source of non-adiabatic effects, the degree of orientation in non-parallel dc and ac fields could be reduced. In this work, we have shown that for parallel fields, the avoided crossing among states with the same symmetry are passed, in general, diabatically for many field configurations. Thus, a time-dependent description will allow us to revise our prediction that in titled fields the avoided crossings among states with the same (different) field-free value of M are crossed adiabatically (diabatically) [24].

ACKNOWLEDGMENTS

We would like to thank Jochen Küpper and Henrik Stapelfeldt for fruitful discussions, and Hans-Dieter Meyer for providing us the code of the short iterative Lanczos algorithm. Financial support by the Spanish project FIS2011-24540 (MICINN), the Grants P11-FQM-7276 and FQM-4643 (Junta de Andalucía), and Andalu-

sian research group FQM-207 is gratefully appreciated. This research was supported in part by the National Sci-

ence Foundation under Grant No. PHY11-25915. J.J.O. acknowledges the support of ME under the program FPU.

-
- [1] P. R. Brooks, *Science* **193**, 11 (1976).
 - [2] P. R. Brooks and E. M. Jones, *J. Chem. Phys.* **45**, 3449 (1966).
 - [3] H. J. Loesch and J. Möller, *J. Chem. Phys.* **97**, 9016 (1992).
 - [4] F. J. Aoiz, B. Friedrich, V. J. Herrero, V. S. Rábanos, and J. E. Verdasco, *Chem. Phys. Lett.* **289**, 132 (1998).
 - [5] V. Aquilanti, M. Bartolomei, F. Pirani, D. Cappelletti, and F. Vecchiocattivi, *Phys. Chem. Chem. Phys.* **7**, 291 (2005).
 - [6] C. Z. Bisgaard, O. J. Clarkin, G. Wu, A. M. D. Lee, O. Gessner, C. C. Hayden, and A. Stolow, *Science* **323**, 1464 (2009).
 - [7] L. Holmegaard, J. L. Hansen, L. Kalhøj, S. L. Kragh, H. Stapelfeldt, F. Filsinger, J. Küpper, G. Meijer, D. Dimitrovski, M. Abu-samha, et al., *Nat. Phys.* **6**, 428 (2010).
 - [8] J. L. Hansen, H. Stapelfeldt, D. Dimitrovski, M. Abu-samha, C. P. J. Martiny, and L. B. Madsen, *Phys. Rev. Lett.* **106**, 073001 (2011).
 - [9] E. Frumker, C. T. Hebeisen, N. Kajumba, J. B. Bertrand, H. J. Wörner, M. Spanner, D. M. Villeneuve, A. Naumov, and P. B. Corkum, *Phys. Rev. Lett.* **109**, 113901 (2012).
 - [10] P. M. Kraus, A. Rupenyan, and H. J. Wörner, *Phys. Rev. Lett.* **109**, 233903 (2012).
 - [11] L. S. Spector, M. Artamonov, S. Miyabe, T. Martinez, T. Seideman, M. Guehr, and P. H. Bucksbaum (2012), arXiv:1207.2517.
 - [12] S. Stolte, *Atomic and Molecular Beam Methods* (Oxford University Press, New York, 1988).
 - [13] H. J. Loesch and A. Remscheid, *J. Chem. Phys.* **93**, 4779 (1990).
 - [14] B. Friedrich and D. R. Herschbach, *Nature* **353**, 412 (1991).
 - [15] B. Friedrich, D. P. Pullman, and D. R. Herschbach, *J. Phys. Chem.* **95**, 8118 (1991).
 - [16] P. A. Block, E. J. Bohac, and R. E. Miller, *Phys. Rev. Lett.* **68**, 1303 (1992).
 - [17] B. Friedrich, H. G. Rubahn, and N. Sathyamurthy, *Phys. Rev. Lett.* **69**, 2487 (1992).
 - [18] A. Slenczka, B. Friedrich, and D. Herschbach, *Phys. Rev. Lett.* **72**, 1806 (1994).
 - [19] B. Friedrich and D. R. Herschbach, *J. Chem. Phys.* **111**, 6157 (1999).
 - [20] B. Friedrich and D. Herschbach, *J. Phys. Chem. A* **103**, 10280 (1999).
 - [21] L. Holmegaard, J. H. Nielsen, I. Nevo, H. Stapelfeldt, F. Filsinger, J. Küpper, and G. Meijer, *Phys. Rev. Lett.* **102**, 023001 (2009).
 - [22] I. Nevo, L. Holmegaard, J. Nielsen, J. L. Hansen, H. Stapelfeldt, F. Filsinger, G. Meijer, and J. Küpper, *Phys. Chem. Chem. Phys.* **11**, 9912 (2009).
 - [23] T. Seideman and E. Hamilton, *Adv. Atom. Mol. Opt. Phys.* **52**, 289 (2006).
 - [24] J. J. Omiste, M. Gärttner, P. Schmelcher, R. González-Férez, L. Holmegaard, J. H. Nielsen, H. Stapelfeldt, and J. Küpper, *Phys. Chem. Chem. Phys.* **13**, 18815 (2011).
 - [25] J. H. Nielsen, H. Stapelfeldt, J. Küpper, B. Friedrich, J. J. Omiste, and R. González-Férez, *Phys. Rev. Lett.* **108**, 193001 (2012).
 - [26] J. J. Omiste and R. González-Férez, *Phys. Rev. A* **86**, 043437 (2012).
 - [27] F. Filsinger, J. Küpper, G. Meijer, L. Holmegaard, J. H. Nielsen, I. Nevo, J. L. Hansen, and H. Stapelfeldt, *J. Chem. Phys.* **131**, 064309 (2009).
 - [28] J. Bulthuis, J. Miller, and H. J. Loesch, *J. Phys. Chem. A* **101**, 7684 (1997).
 - [29] R. Escribano, B. Maté, F. Ortigoso, and J. Ortigoso, *Phys. Rev. A* **62**, 023407 (2000).
 - [30] A. Schwettman, J. Franklin, K. R. Overstreet, and J. P. Shaffer, *J. Chem. Phys.* **123**, 194305 (2005).
 - [31] K. Wohlfart, F. Filsinger, F. Grätz, J. Küpper, and G. Meijer, *Phys. Rev. A* **78**, 033421 (2008).
 - [32] M. Kirste, B. G. Sartakov, M. Schnell, and G. Meijer, *Phys. Rev. A* **79**, 051401 (2009).
 - [33] S. A. Meek, H. Conrad, and G. Meijer, *Science* **324**, 1699 (2009).
 - [34] T. E. Wall, S. K. Tokunaga, E. A. Hinds, and M. R. Tarbutt, *Phys. Rev. A* **81**, 033414 (2010).
 - [35] R. N. Zare, *Angular Momentum: Understanding Spatial Aspects in Chemistry and Physics* (John Wiley and Sons, New York, 1988).
 - [36] G. W. King, R. M. Hainer, and P. C. Cross, *J. Chem. Phys.* **11**, 27 (1943).
 - [37] M. Beck, A. Jäckle, G. Worth, and H.-D. Meyer, *Physics Reports* **324**, 1 (2000).
 - [38] J. J. Omiste, R. González-Férez, and P. Schmelcher, *J. Chem. Phys.* **135**, 064310 (2011).
 - [39] L. B. Ballentine, *Quantum Mechanics: A Modern Development* (World Scientific, Singapore, 1998).
 - [40] K. Wohlfart, M. Schnell, J.-U. Grabow, and J. Küpper, *J. Mol. Spectrosc.* **247**, 119 (2007).
 - [41] J. L. Hansen, L. Holmegaard, L. Kalhøj, S. L. Kragh, H. Stapelfeldt, F. Filsinger, G. Meijer, J. Küpper, D. Dimitrovski, M. Abu-samha, et al., *Phys. Rev. A* **83**, 023406 (2011).
 - [42] Y. Sugawara, A. Goban, S. Minemoto, and H. Sakai, *Phys. Rev. A* **77**, 031403(R) (2008).
 - [43] M. Muramatsu, M. Hita, S. Minemoto, and H. Sakai, *Phys. Rev. A* **79**, 011403(R) (2009).